MNRAS **000**, 1–15 (2019) Preprint April 4, 2022 Compiled using MNRAS LATEX style file v3.0

The role of a top-heavy integrated galactic IMF on the chemical evolution of high-redshift starbursts

M. Palla[1,2]★, F. Calura[3], X. L. Fan[4], F. Matteucci[1,5,6], F. Vincenzo[7] and E. Lacchin[1]

[1] *Dipartimento di Fisica, Sezione di Astronomia, Universitá degli Studi di Trieste, via G. B. Tiepolo 11, I-34131, Trieste, Italy*
[2] *IFPU - Institute for Fundamental Physics of the Universe, Via Beirut 2, I-34014, Trieste, Italy*
[3] *INAF, Osservatorio Astronomico di Bologna, via P. Gobetti 93/3, I-40129, Bologna, Italy*
[4] *School of Physics and Technology, Wuhan University, 430072, Wuhan, Hubei, 430205, China*
[5] *INAF, Osservatorio Astronomico di Trieste, via G. B. Tiepolo 11, I-34131, Trieste, Italy*
[6] *INFN, Sezione di Trieste, via A. Valerio 2, I-34100, Trieste, Italy*
[7] *School of Physics and Astronomy, University of Birmingham, Edgbaston, B15 2TT, UK*

arXiv:1908.06832v1 [astro-ph.GA] 19 Aug 2019

Accepted XXX. Received YYY; in original form ZZZ

ABSTRACT

We apply a top-heavy integrated galactic initial mass function (IGIMF) to the chemical evolution of spheroids and compare our results with high redshift starburst galaxies. These objects are, in fact, very likely to be elliptical galaxies suffering their main burst of star formation. These bursts are very intense and more massive objects suffer more intense star formation than less massive ones (downsizing in star formation). The high star formation rate produces a galactic wind, due to stellar feedback, and devoids the galaxy of the gas residual from star formation. This happens sooner for more massive galaxies (inverse wind model), ensuring the reproduction of the mass-Z relation and the [α/Fe]-mass relation in local ellipticals. We compute the chemical evolution, including also a detailed dust treatment, of α-elements, Fe, C and N, and we compare our results with the available data for high redshift starburst galaxies. Our main conclusions are: i) the top-heavy IGIMF enhances the rate of star formation; in particular, different β (parameter related to the slope of the embedded cluster mass function) determine different times for the occurrence of the galactic wind. The $\beta = 1$ value is rejected since it produces models which do not satisfy the condition of the inverse wind model, whereas for $\beta > 1$ the inverse wind is preserved. ii) Abundance data are in general better reproduced by models adopting the top-heavy IGIMF than a classical Salpeter IMF. iii) The abundance ratios of refractory elements relative to Fe can be explained only by assuming the presence of dust.

Key words: stars: luminosity function, mass function - galaxies: starburst - galaxies: evolution - galaxies: abundances - ISM: dust, extinction

1 INTRODUCTION

The initial mass function (IMF) is known to influence most observable properties of stellar populations, by determining the low to high stellar mass ratio. The massive stars are known to be the main producers of α-elements[1] over short ($\leq 30 Myr$) timescales. On the opposite side, the bulk of Fe in a galaxy is produced via Type Ia SNe over timescales that can even reach or exceed the Hubble time (Matteucci & Greggio 1986; Matteucci & Recchi 2001). This difference in production channels and time-scales, when combined with the star formation history of a galaxy, leaves a characteristic mark on abundance ratios which may allow us to reconstruct the formation history from observations (e.g. Matteucci 2003; Matteucci 2012). Besides the chemical evolution, many other properties of a galaxy are strictly related to the IMF: present time stellar mass (Kennicutt 1998), integrated light of galaxies (Conroy & van Dokkum 2012b), energetic feedback from star formation episodes are just examples of that.

At present, a complete theory able to explain the origin of the IMF does not exist. Another fundamental issue yet to be clarified concerns the universality of the IMF, as in principle in the local Universe it could be different from high redshift galaxies (e.g. Larson 1998), which are likely to be characterised by much different physical conditions.

★ E-mail: marco.ball94@gmail.com

[1] Elements characterised by capture of α particles. Examples are O, Mg, Si, S, Ca.

© 2019 The Authors

In this uncertain scenario it enters the integrated galactic initial mass function (IGIMF) theory. The IGIMF theory is based on a few basic empirical evidences related to the birth of stars in local star-forming environments, which include the fact that: (i) stars form only in clusters (Lada & Lada 2003); (ii) within each stellar cluster, the IMF is observed to be universal and well approximated by a multiple power-law form (Massey & Hunter 1998; Pflamm-Altenburg et al. 2007); (iii) stellar clusters are apparently distributed according to a single-slope power law (Lada & Lada 2003) and (iv) the upper mass end of the embedded cluster mass function has been found to depend on the star formation rate (SFR) of the galaxy (Weidner & Kroupa 2004). The main direct consequence of these evidences is that the integrated IMF in disc galaxies (such as the Milky Way) is generally steeper than the stellar IMF within each single star cluster (Kroupa & Weidner 2003).
Later, Weidner et al. (2011) extended the IGIMF theory to systems characterised by high star formation rates (SFR> $10 M_{\odot} yr^{-1}$), showing that in the most intensely star-forming objects, i.e. in very massive and compact systems, the resulting IMF becomes top-heavy, with extreme consequences on supernova feedback and chemical enrichment.

These particular aspects are the motivation of the present paper, where we aim at testing the effects of a top-heavy IGIMF on the chemical evolution of the starbursts observed at high-redshift.
As a matter of fact, various studies indicate that a high-redshift top-heavy IMF seems to be required to explain several properties of local and distant galaxies, including the observed evolution of the optical luminosity density (Larson 1998), the integrated [α/Fe] ratios (Calura & Menci 2009; De Masi et al. 2018) and the colour-luminosity relation (Gibson & Matteucci 1997) in local spheroids, the observed galaxy number counts in the infrared band and at submillimetric wavelengths (Baugh et al. 2005), the isotopic ratios in high-z starbursts (Zhang et al. 2018) and the discrepancy between the observed present-day stellar mass density and the integral of the comoving SFR density (Davé 2008). In order to conciliate other indications in early type galaxies (e.g. Cenarro et al. 2003; Conroy & van Dokkum 2012a,2012b; La Barbera et al. 2013) suggesting a bottom-heavy IMF, Weidner et al. (2013) and Ferreras et al. (2015) proposed also a time-dependent form of the IMF, switching from a top-heavier form during the initial burst of star formation to a bottom-heavier one at later times.

To test our models, we compare abundance patterns with data coming from high-redshift objects with characteristics (e.g. mass, SFR) similar to the models. High resolution spectrographs, in fact, have determined a great development in the study of chemical abundances in high-redshift systems: chemical abundances derived using either emission or absorption line spectroscopy have allowed us to gain crucial constraints on the physical properties of high-redshift systems such as Lyman Break Galaxies (LBGs). We include in the models also dust differential depletion. This feature in fact can help to explain abundances of refractory elements (i.e. elements severely depleted from the gas phase) in such objects. As a matter of fact, previous chemical evolution models without it fail to reproduce [α/Fe] ratios in objects of the class of our analysis (Matteucci & Pipino 2002; Pipino et al. 2011 with MS 1512-cB58 LBG).

The present work follows various studies carried on in the last few years, aimed at assessing the chemical evolution effects of the IGIMF in various environments characterised by rather different star formation histories, i.e. the solar neighbourhood (Calura et al. 2010), dwarf galaxies (Vincenzo et al. 2015) and local elliptical galaxies (Recchi et al. 2009; De Masi et al. 2018; Yan et al. 2019). It should be noted that the present paper is the first introducing the effects of dust differential depletion in chemical evolution models adopting an IGIMF.

The paper is organized as follows: in Section 2, we describe the IGIMF theory and chemical evolution model adopted in this work. Our observational data, results and discussions are presented in Section 3. Finally, some conclusions are drawn in Section 4.

2 MODELS

In this Section, we are describing the integrated galactic initial mass function (IGIMF) theory and the main features of the chemical evolution model adopted in this paper.

2.1 IGIMF

Following the works of Kroupa & Weidner (2003) and Weidner & Kroupa (2005), the IGIMF is defined by weighting the canonical IMF, $\phi(m)$, with the mass distribution of the stellar clusters (called embedded cluster mass function, ECMF), $\xi_{ecl}(M_{ecl})$. As a matter of fact, IGIMF theory starts from the assumption that all the star formation process in a galaxy takes place in stellar clusters. In particular, we can write:

$$\xi_{\rm IGIMF}(m,t) = \\ = \int_{M_{\rm ecl,min}}^{M_{\rm ecl,max}(\psi(t))} \phi(m \leq m_{\rm max}(M_{\rm ecl}))\, \xi_{ecl}(M_{ecl})\, dM_{\rm ecl}, \quad (1)$$

where M_{ecl} is the cluster mass. To make the IGIMF comparable with a classical Salpeter (1955) IMF, we normalize it in mass to unity, in this way (see De Masi et al. 2018)

$$\int_{m_{min}}^{m_{max}} m\, \xi_{\rm IGIMF}(m,t)\, dm = 1.$$

As it can be seen from Equation (1), the IGIMF adopted in this work has a time dependence, which is due to the SFR $\psi(t)$ of the parent galaxy, following the model of Weidner et al. (2011) (hereafter W11). We now list the assumptions, based on observations, on which the IGIMF adopted here is based.

(i) The ECMF is represented by a single-slope power law:

$$\xi_{\rm ecl}(M_{\rm ecl}) \propto \left(\frac{M_{\rm ecl}}{M_{\rm ecl,max}}\right)^{-\beta}, \quad (2)$$

where the slope β can be varied from $\beta = 2.35$ to $\beta = 0.5$. Concerning the mass range of $M_{\rm ecl}$ spanned by the ECMF, we assume $M_{\rm ecl,min} = 10^3 M_{\odot}$ according to W11. This choice is due to the fact that under high SFRs, low mass molecular cloud cores may be suppressed for the intense stellar feedback. At the same time, it must be said that for slopes $\beta \leq 2$ (as adopted in this paper) the ECMF is not very sensitive to

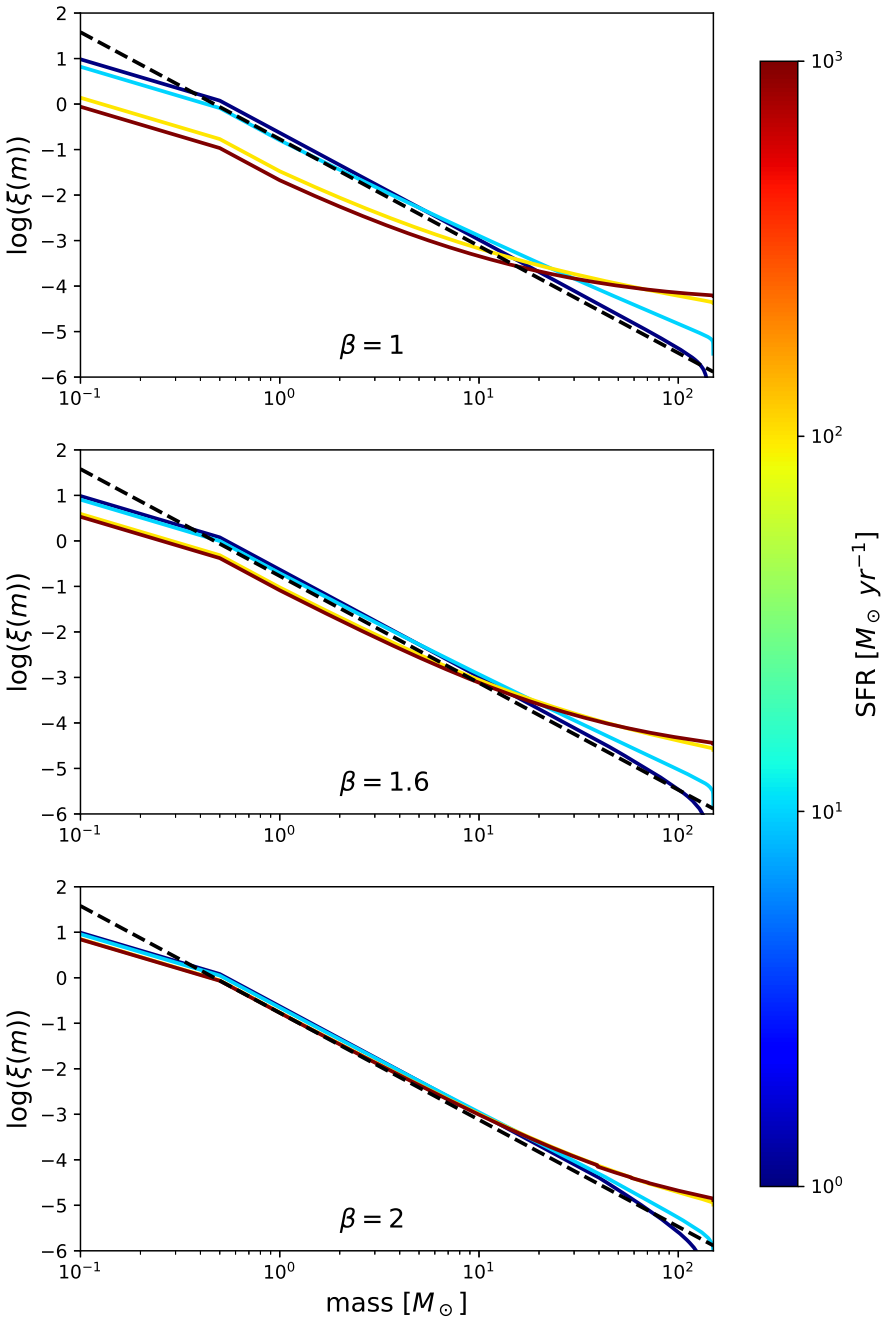

Figure 1. Behaviour of the IGIMF adopted in this paper as a function of stellar mass and SFR. Upper panel: β = 1; central panel: β = 1.6; lower panel: β = 2. In each panel, the four solid lines are the IGIMFs computed considering SFR=$1M_\odot\,yr^{-1}$,$10M_\odot\,yr^{-1}$, $100M_\odot\,yr^{-1}$, $1000M_\odot\,yr^{-1}$. The black dashed lines indicate the Salpeter (1955) IMF.

the value of $M_{\rm ecl,min}$, since it is dominated by massive clusters. About the upper mass limit $M_{\rm ecl,max}$ we follow Weidner & Kroupa (2004) expression:

$$M_{\rm ecl,max} = 8.5 \cdot 10^4 \left(\frac{\psi(t)}{M_\odot\, yr^{-1}}\right) M_\odot, \tag{3}$$

which holds for both low and high SFRs (Bastian 2008). We fix a maximum value for this upper mass limit at $10^7 M_\odot$, coherently with Weidner & Kroupa (2004).

(ii) Within each embedded stellar cluster of a given mass $M_{\rm ecl}$, the IMF is assumed to be invariant. Following W11, we adopt the multi-component canonical IMF (Kroupa 2001, 2002), which in its general form is expressed as:

$$\phi(m) = k \begin{cases} k' \left(\frac{m}{m_{\rm H}}\right)^{-\alpha_0} \\ \left(\frac{m}{m_{\rm H}}\right)^{-\alpha_1} \\ \left(\frac{m_0}{m_{\rm H}}\right)^{-\alpha_1} \left(\frac{m}{m_0}\right)^{-\alpha_2} \\ \left(\frac{m_0}{m_{\rm H}}\right)^{-\alpha_1} \left(\frac{m_1}{m_0}\right)^{-\alpha_2} \left(\frac{m}{m_1}\right)^{-\alpha_3} \end{cases}, \tag{4}$$

with the following exponent values:

$$\begin{array}{lll} \alpha_0 = +0.30 & , & 0.01 \le m/M_\odot < 0.08, \\ \alpha_1 = +1.30 & , & 0.08 \le m/M_\odot < 0.50, \\ \alpha_2 = +2.35 & , & 0.50 \le m/M_\odot < 1.00, \\ \alpha_3 = +2.35 & , & 1.00 \le m/M_\odot \le m_{\rm max}. \end{array} \tag{5}$$

In previous chemical evolution studies involving the IGIMF formalism, the quantity α_3 has been kept equal to 2.35, independently from the cluster mass (e.g. Recchi et al. 2009, Calura et al. 2010). In this paper instead, in order to follow W11, for cluster with masses $M_{\rm ecl} > 2 \cdot 10^5 M_\odot$, the exponent α_3 is parametrised as:

$$\alpha_3(M_{\rm ecl}) = \begin{cases} -1.67\ \log_{10}\left(\frac{M_{\rm ecl}}{10^6 M_\odot}\right) + 1.05\ , M_{\rm ecl} \le 10^6 M_\odot, \\ +1 \qquad\qquad\qquad\qquad\qquad\qquad , M_{\rm ecl} > 10^6 M_\odot. \end{cases} \tag{6}$$

As discussed in Marks et al. (2012), in fact, various features of some Galactic globular clusters (GCs) can be accounted for only with a top-heavy stellar IMF. On the other hand, the possibility of a top-heavy IMF is contemplated also in current scenarios for the birth of multiple stellar generations in GCs (e.g. D'Antona & Caloi 2004; D'Ercole et al. 2008), necessary to explain the observed abundances within them. Regarding the upper stellar mass limit $m_{\rm max}$, this is computed according to the mass of the embedded cluster $M_{\rm ecl}$, but in any case is considered smaller or equal than $150 M_\odot$ (see Weidner & Kroupa 2004 for more details).

In the present study, it is not taken into account a metallicity effect of the IGIMF, as it has been done in some previous works (e.g. Recchi et al. 2014; Vincenzo et al. 2015; Yan et al. 2019). The adoption of a metallicity dependent IGIMF in high redshift starburst galaxies will be the subject of a future work.

2.1.1 IGIMF choice and behaviour

In Figure 1, we show the IGIMF behaviour obtained using the described prescriptions for different values of the SFR. As can be seen from the Figure, we select to test three values of β among those adopted in W11: $\beta = 1$, $\beta = 1.6$ and $\beta = 2$.

We do not consider in this study the extreme values of $\beta = 0.5$ and $\beta = 2.35$. On one hand, in fact, still adopting an ECMF with $\beta = 1$ we obtain for $\psi \gtrsim 10 M_\odot yr^{-1}$ an IMF that is already comparable with the single-slope one of Gibson & Matteucci (1997), known to be a quite extreme top-heavy one (with x=0.8 over the whole stellar mass range). On the other side, since we want to explore the IGIMF in a top-heavy regime, a β disfavouring too much massive clusters formation (and consequently, massive stars formation) seemed not appropriate for our final goal.

Coming back to Figure 1, we can see that the IGIMFs calculated at low SFRs ($1 M_\odot\, yr^{-1}$) show an uniform decline with mass from the knee located at m_0, which follow approximately a power law until $100 M_\odot$. In general, it is visible that for higher SFRs the slope of the IGIMF becomes flatter, favouring massive stars. This is due to the increase of $M_{ecl,max}$ value increasing the SFR. In particular, we see a stronger dependence on the SFR lowering the β value. This because for flatter ECMF (i.e. lower β), the embedded cluster distribution is biased towards higher masses, thus enhancing the importance of $M_{ecl,max}$ value. Thanks to this, the IGIMF slopes for values of $\psi >> 1 M_\odot\, yr^{-1}$ remain comparable with the one of the Salpeter (1955) only for the steepest ECMF ($\beta = 2$).

2.2 Chemical evolution model

The model used in this work was originally designed to study the evolution of elliptical galaxies (Matteucci 1994; Pipino et al. 2011; Calura et al. 2014; De Masi et al. 2018). For further details on the chemical evolution model, we refer the reader to Pipino et al. (2011).

In our scheme, elliptical galaxies form from the rapid collapse of a gas cloud with primordial chemical composition, described by an exponential infall law. After the initial collapse, the galaxy is allowed to evolve as an 'open box' into the potential well of a dark matter halo. The rapid collapse triggers an intense and rapid star formation (SF) process, i.e. a starburst, which lasts until a galactic wind, powered by the thermal energy injected by stellar winds and supernovae (SNe) explosions, occurs. After that time, the galaxy evolves passively, i.e. with no more SF.

In this scenario, the evolution of a given chemical element i is described by:

$$\dot{G}_i = -\psi(t) X_i(t) + R_i(t) + \dot{G}_{i,inf} - \dot{G}_{i,out} \tag{7}$$

where $G_i(t) = X_i(t)\, G(t)$ is the gas mass in the form of an element i normalised to the total baryonic mass M_{lum} and $G(t) = M_{gas}(t)/M_{lum}$ is the fractional mass of gas present in the galaxy at the time t. The quantity $X_i(t) = G_i(t)/G(t)$ represents the abundance fraction in mass of a given element i, where the summation over all elements in the gas mixture being equal to unity. $\psi(t)$, as we have already mentioned, is the star formation rate, i.e. the amount of gas turning into stars per unit time.

$R_i(t)$ represents the returned fraction of matter in the form of an element i that the stars eject into the ISM through stellar winds and supernova explosions. This term takes into account the different nucleosynthesis prescriptions for the specific element i. It includes the contribution from single low-intermediate mass stars (LIMS), characterised by initial masses $m < 8 M_\odot$, from core collapse (CC) SNe (Type II and Ib/c), originating from the explosion of massive stars with initial mass of $m > 8 M_\odot$, and from Type Ia SNe, for which

we assume the single-degenerate (SD) scenario. In this scenario, a C-O white dwarf in a binary system accretes mass from a non-degenerate companion until it reaches the Chandrasekhar mass ($\sim 1.44 M_{\odot}$) and explodes via C-deflagration, leaving no remnant. Stellar yields for this work are taken from van den Hoek & Groenewegen (1997) (LIMS), François et al. (2004) (revised version of Woosley & Weaver 1995, for massive stars; for nitrogen see 3.4.1) and Iwamoto et al. (1999) (Type Ia SNe). The fraction of stars in binary systems able to originate Type Ia SNe is fixed at a value able to reproduce the present day type Ia SN rate observed in local ellipticals using a Salpeter (1955) IMF (Matteucci & Recchi 2001; Calura & Matteucci 2006; Pipino & Matteucci 2011). We do not vary it for the IMFs adopted here, in order to avoid degeneracies in the models. Moreover, a variation in this parameter impacts very little or none our analysis on abundance behaviour.

In Equation 7, the two terms $\dot{G}_{i,inf}$ and $\dot{G}_{i,out}$ account for the infall of external gas and for galactic winds, respectively. For the infall, we assume an exponential law

$$\dot{G}_{i,inf} \propto X_{i,inf} \exp(-t/\tau_{inf}), \tag{8}$$

where $X_{i,inf}$ describes the chemical composition of the infalling gas, assumed to be primordial. The quantity τ_{inf} is the infall timescale. Concerning the galactic wind, its occurrence is given by the condition that that the thermal energy of the ISM, due to feedback from SNe and stellar winds from massive stars, is larger or equal to gas binding energy. The feedback prescriptions assumed here are the same as in De Masi et al. (2018): in particular, we assume that only a small fraction of the initial blast wave energy of CC-SNe, $E_o = 10^{51}$erg is stored in the ISM, whereas all the initial blast wave energy of Type Ia SNe (the same as for CC-SNe) is stored in the ISM, as suggested by Recchi et al. (2001). This is due to the fact that when Type Ia SNe explode, the ISM is already hot because of the explosion of previous CC-SNe. Moreover, we assume that stellar winds by massive stars can inject into the ISM ~3% of the typical energy of stellar winds ($\sim 10^{49}$ erg, see Bradamante et al. 1998 for details). Related to the wind occurrence, the dark matter halo is assumed ten times more massive than the luminous mass, with its core radius being also ten times larger than the effective radius, in agreement with previous papers (Matteucci 1994; Pipino & Matteucci 2004; De Masi et al. 2018), where details can be found.

In this paper, the SFR is calculated as:

$$\psi(t) = \nu G(t), \tag{9}$$

i.e. it is assumed to be proportional to the gas mass via a constant ν, the star formation efficiency, according to the Schmidt-Kennicutt law (Schmidt 1959; Kennicutt 1998). The star formation efficiency is allowed to vary as a function of the mass, in order to reproduce the "inverse wind model" of Matteucci (1994), which reproduces the "downsizing" behaviour of galaxies. In other words, increasing the SF efficiency produces a galactic wind occurring at earlier times in the more massive systems, thus producing higher [α/Fe] ratios in the dominant stellar population of the most massive galaxies, in agreement with observations (see also De Masi et al. 2018).

Another fundamental quantity in the model is the already discussed stellar IMF. In the remainder of the paper, we will compare the results obtained with the IGIMF described in Section 2.1 with those obtained with a standard Salpeter (1955) IMF, expressed by a single power law as $\xi(m) \propto m^{-2.35}$.

Table 1. Main parameters assumed for our chemical evolution models for starburst galaxies.

Model name	M_{lum} ($M_{\odot}$)	R_{eff} (kpc)	ν (Gyr^{-1})	τ_{inf} (Gyr)
M3E10	3×10^{10}	2	5	0.5
M1E11	1×10^{11}	3	10	0.4
M1E12	1×10^{12}	10	20	0.2

The main features of the models used in this paper are summarised in Table 1. In the first column, the name of the model is shown. The second column shows the adopted total baryonic mass of the models. The third, the fourth and the fifth columns indicate for each model the adopted effective radius, the star formation efficiency and the infall timescale.

2.2.1 *Dust evolution model*

The chemical evolution model also follows in detail the various processes that influence dust evolution. We adopted the same formalism used in previous works on chemical evolution models with dust (e.g. Dwek 1998; Calura et al. 2008; Gioannini et al. 2017; Vladilo et al. 2018). For further details on the dust evolution model and its prescriptions, we refer the reader to Palla et al. (2019).

For a specific element i in the dust phase we have:

$$\begin{aligned}\dot{G}_{i,dust} = &-\psi(t)X_{i,dust}(t) + \delta_i R_i(t) + G_{i,dust}(t)/\tau_{i,accr} + \\ &-G_{i,dust}(t)/\tau_{i,destr} - \dot{G}_{i,dust,out}\end{aligned} \tag{10}$$

where $G_{i,dust}$ and $X_{i,dust}$ are the same of Equation (7), but for only the dust phase. This last Equation takes into account dust production from AGB stars and core-collapse SNe ($\delta_i R_i$), accretion in molecular clouds ($G_{i,dust}/\tau_{i,accr}$), destruction by SNe shocks ($G_{i,dust}/\tau_{i,destr}$). To compute the terms, we adopt detailed prescriptions from literature. For dust production, we use tested (e.g. Ginolfi et al. 2018), metallicity-dependent prescriptions reported by Bianchi & Schneider (2007) (for CC-SNe) and Dell'Agli et al. (2017) (for AGB stars). For the processes of accretion and destruction by SNe, we adopt the metallicity-dependent timescales $\tau_{i,accr}$, $\tau_{i,destr}$ from Asano et al. (2013). For the wind, we assume that dust and gas in the ISM are coupled. The main reason is that we are focusing on the evolution before the onset of the galactic wind.

At variance with previous chemical evolution works on elliptical galaxies (Pipino et al. 2011; Grieco et al. 2014), we assume that Type Ia SNe do not produce dust. This assumption is supported from either the theoretical and the observational sides (Nozawa et al. 2011; Gomez et al. 2012).

3 RESULTS

In this Section, our aim is to test the effects of the IGIMF on the main global properties of galaxies of various masses,

Table 2. Features of starburst galaxies included in our sample. Objects above (below) the line are lensed galaxies (stacked spectra).

Object	Redshift	SFR ($M_\odot/yr$)	M_* ($M_\odot$)	Abundances	Notes	References
MS 1512-cB58	2.7276	~25-~150	10^{10}	O,N,Fe,Mg,Si	(1),(2)	Pettini et al.(2000, 2001, 2002); Teplitz et al. (2000); Siana et al. (2008)
SGAS J105039.6+001730	3.6252	~50-~80	$10^{9.5}$	O,N,C	(1),(3)	Bayliss et al. (2014)
RCSGA 032727-132609	1.7037	~210	10^{10}	O,N	(3)	Wuyts et al. (2010); Rigby et al. (2011)
SMACS J0304.3-4402	1.96	~30-~90	$10^{10.57}$	O,N	(1),(3)	Christensen et al.(2012a, 2012b)
SMACS J2031.8-4036	3.51	~15-~25	$10^{9.16}$	O,C	(1),(3)	Christensen et al.(2012a, 2012b)
8 o'clock arc	2.7350	~270	$10^{11.6}$	Fe,Si	(4)	Dessauges-Zavadsky et al. (2010); Finkelstein et al. (2009)
KBSS-LM1 Composite	2.396±0.111	29.2±17.6	$10^{9.8\pm0.3}$	O,N,C	(3),(5)	Steidel et al. (2016)
Shapley LBG Composite	~3	-	-	O,C	(6)	Shapley et al. (2003); Pettini et al. (2001)

(1) different SFR values are coming from different SFR indicators (e.g. Hα, UV, IR, [OII]) used in the studies; (2) abundances from absorption lines, except O estimated through R_{23} indicator; (3) abundances from emission lines (O from direct measures); (4) abundances from absorption lines; (5) errors are interquartile intervals on median values, except for redshift (rms on medium values); (6) abundances from emission lines (O derived by [OIII], [OII] and Hβ line strengths)

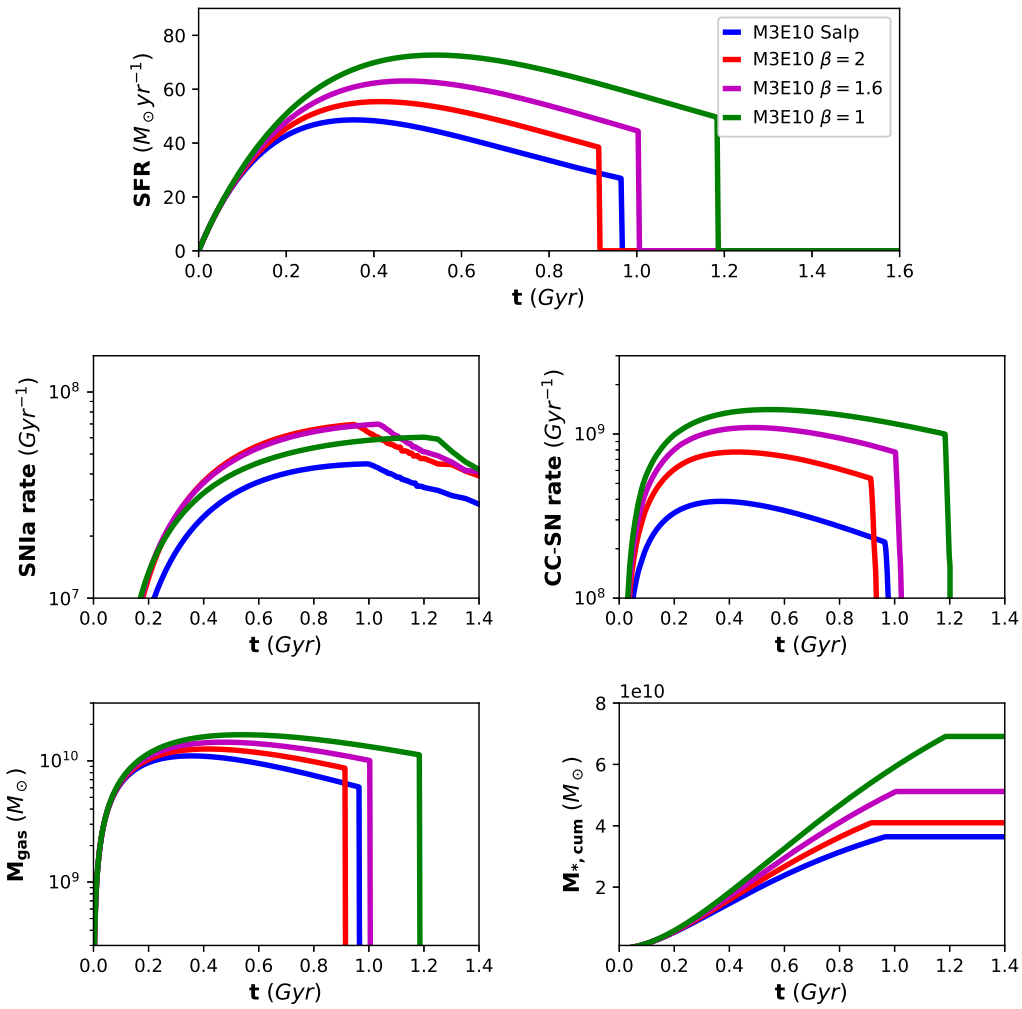

Figure 2. From top to bottom, left to right: time evolution of the SFRs, Type Ia SN rates, CC-SN rates, gas mass and cumulative stellar mass. Lines are calculated for the M3E10 model (see Table 1) with a Salpeter (1955) IMF (blue lines) and assuming an IGIMF calculated for β = 1 (green lines), β = 1.6 (magenta lines) and β = 2 (red lines). The sharp truncation in the SFR, CC-SN rate and gas mass are due to the onset of the galactic wind which devoids the galaxy from the residual gas.

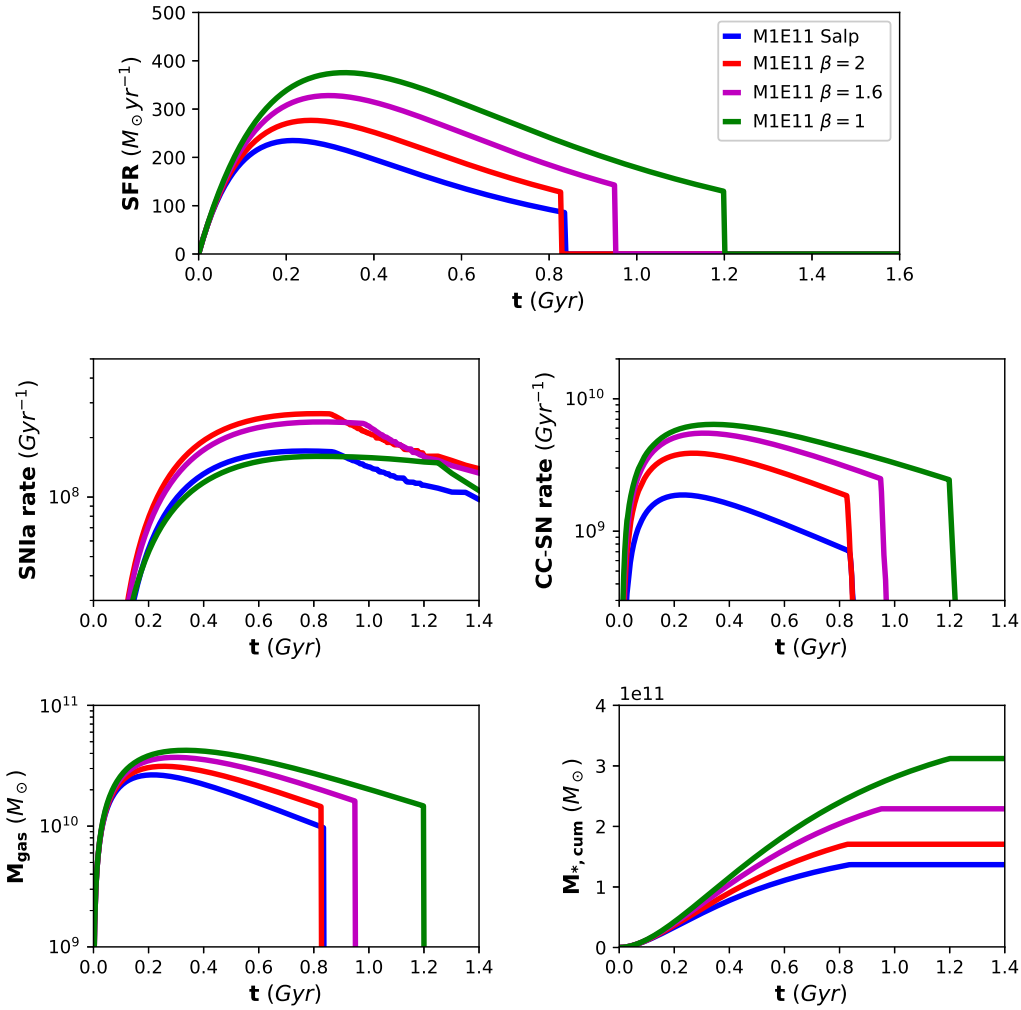

Figure 3. From top to bottom, left to right: time evolution of the SFRs, Type Ia SN rates, CC-SN rates, gas mass and cumulative stellar mass. Lines are calculated for the M1E11 model (see Table 1) with a Salpeter (1955) IMF (blue lines) and assuming an IGIMF calculated for $\beta = 1$ (green lines), $\beta = 1.6$ (magenta lines) and $\beta = 2$ (red lines).

including the star formation history, the SN rates, the evolution of the gas and stellar mass budget and the metal abundances. The calculated elemental abundance ratios will also be compared to the values observed in high redshift starburst galaxies spectra. This comparison can be used also to better constrain the nature of the galaxies included in the sample.

3.1 Observational data

In Table 2 are listed the targets selected for this study with their main features (redshift, SFR, stellar mass and abundances measured).

We consider mainly lensed LBGs (MS 1512-cB58, SGAS J105039.6, 8 o'clock arc) and Ly-α emitters (SMACS J0304.3, SMACS J2031.8). As a matter of fact, the lensing magnification (up to 50, Christensen et al. 2012b) allows to perform high quality spectroscopy from which physical properties and abundances can be derived (Bayliss et al. 2014 and references therein). In the lower part of Table 2 are considered composite spectra. The two objects considered have however suitable characteristics to be included in the sample. The one from Steidel et al. 2016 obeys to the criterion adopted for the sample ($z \gtrsim 2$, $M_* \gtrsim 10^9 M_\odot$, SFR$\gtrsim 20$), whereas the second one is composed by LBGs only, already identified as the progenitors of local spheroids (e.g. Matteucci & Pipino 2002) . The reason to include these stacked spectra is to better constrain our models: as it can be seen from the Table, in fact, only few studies of high redshift starbursts are available with published abundance ratios. Most of the studies, in fact, give only a log(O/H) estimation.

3.2 The effects of the IGIMF on the galactic star formation history

In Figures 2-4 we show the impact of the IMF on the evolution of the SFR, of the Type Ia and CC-SN rates, of the gas and cumulative stellar mass for models of starbursts presented in Table 1.

We remind that all the models reported in Figures 2, 3 and

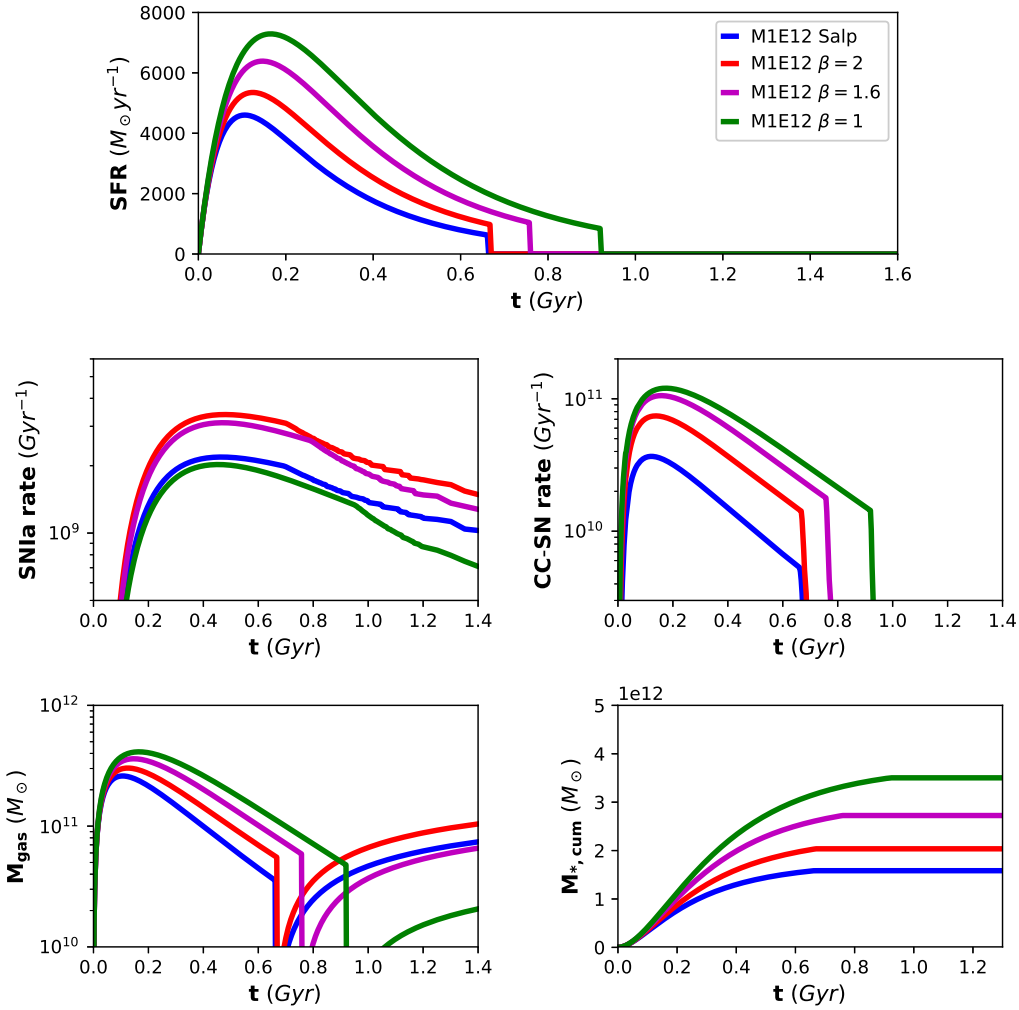

Figure 4. From top to bottom, left to right: time evolution of the SFRs, Type Ia SN rates, CC-SN rates, gas mass and cumulative stellar mass. Lines are calculated for the M1E12 model (see Table 1) with a Salpeter (1955) IMF (blue lines) and assuming an IGIMF calculated for $\beta = 1$ (green lines), $\beta = 1.6$ (magenta lines) and $\beta = 2$ (red lines).

4 are characterised by constant SF efficiencies of 5, 10 and 20 Gyr^{-1}, respectively. Each one of the figures is thus useful to single out the effects of the IMF on the global properties of the galaxy of that particular mass.

The star formation histories reported in Figure 2, 3, 4 show large variations due to the effects of the IMF. The models adopting W11 IGIMF in fact exhibit larger SFR values. This can be explained by the fact that a strong top-heavy IMF implies larger mass ejection rates from evolved massive stellar populations, and consequently larger gas mass reservoirs. Because of the proportionality between SFR and the gass mass, larger SFR values are obtained.
The differences in the star formation histories caused by the IMF determine also when the conditions for the onset of a galactic wind are met, thus the time at which the star formation stops. In particular, in the case $\beta = 1$, in spite of the larger number of CC-SNe ($\propto$SFR), relative to the cases with $\beta > 1$, the galactic wind occurs later because of the larger amount of gas and the relatively moderate feedback from these SNe (see Section 2.2). On the other hand, the rate of Type Ia SN, which instead inject most of their energy into the ISM (Cioffi et al. 1988; Recchi et al. 2001), is lower than rates obtained for the $\beta = 1.6$ and $\beta = 2$ cases. The steepest ECMFs ($\beta = 1.6$ and $\beta = 2$) produce instead earlier winds. In these cases, the gas masses are lower than $\beta = 1$ case and the energetic feedback produced by SNe (CC and Type Ia) exceeds the binding energy earlier.

Comparing Figures 2 and 3, it is worth noting that because of the later occurrence of galactic winds in more massive galaxies, the downsizing in star formation, obtained by Matteucci (1994) by means of the inverse wind model (more massive galaxies have shorter and stronger SF episodes, see also Thomas et al. 2002), cannot be reproduced by models adopting $\beta = 1$ IGIMF. The inverse wind model is able to reproduce the increase of the [α/Fe] with galactic stellar mass in ellipticals. For such a reason, we tend to reject the case of the IGIMF with $\beta = 1$. Matteucci (1994) obtained that effect by increasing the efficiency of SF with galactic stellar mass, as we assume here, and a constant Salpeter (1955) IMF. The inverse wind effect is in fact visible in our Figures for the Salpeter (1955) IMF as well as for the case $\beta = 2$ and $\beta = 1.6$.

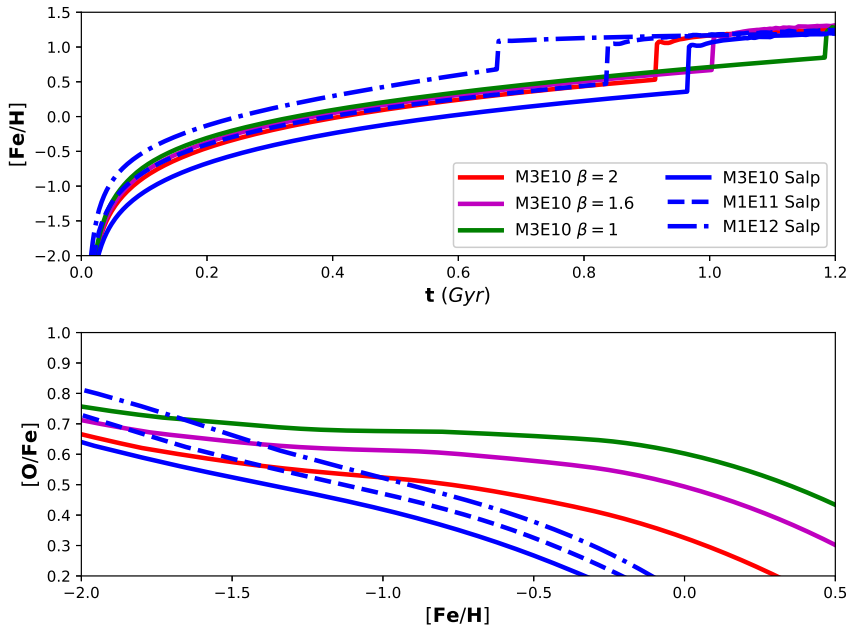

Figure 5. Predicted time evolution of the interstellar [Fe/H] (upper panel) and [O/Fe] vs. [Fe/H] relation (lower panel). Lines are computed for: M3E10 models (solid) with Salpeter (1955) IMF (blue), W11 IGIMF calculated for $\beta = 1$ (green), $\beta = 1.6$ (magenta) and $\beta = 2$ (red); M1E11 model with Salpeter (1955) IMF (dashed blue); M1E12 model with Salpeter (1955) IMF (dash-dotted blue).

In Figure 4 the behaviour of M1E12 models is shown. The general situation is similar to what found for M1E11 models. The similar trends between M1E11 and M1E12 models are explained by the relative similar values for the IGIMFs at $\psi > 100 M_{\odot} yr^{-1}$ (see Figure 1). As a matter of fact, the assumption of an upper mass limit on the maximum mass that a stellar cluster can have ($M_{ecl,max}$), saturates the dependence of the IGIMF on the SFR at high ψ values.

Looking at the lower left panel in Figure 4, it is visible that relatively large amounts of gas are restored into the ISM after the onset of the galactic wind. The same behaviour does not occur for lower mass models. Such a restoration is possible if the total amount of binding energy from stars dying immediately after the occurrence of galactic wind is larger than the energy injected by SNe. After that, the total amount of ISM replaced in the galaxy is related to the death of intermediate and low mass stars ($m < 8 M_{\odot}$), which are the only responsible for the ISM pollution after galactic wind starts (stars with $m > 8 M_{\odot}$ have lifetimes $< 30 Myr$). This last fact is explained by looking at Type Ia SN rates.

3.3 The effects of the IGIMF on chemical abundances

In Figure 5, we show the predicted time evolution of the [Fe/H] (upper panel) and the [O/Fe] vs. [Fe/H] plot (lower panel) computed for all the M3E10 models and the M1E11, M1E12 models with a Salpeter (1955) IMF.

The upper panel shows that, in general, Weidner et al. (2011) IGIMF produces at any time larger [Fe/H][2] values with respect to a Salpeter (1955) IMF. We can also see that lowering the β parameter contributes to a faster chemical enrichment. It is evident that the change of IMF is able to compensate, at least in great part, for the SFR enhancement given by models for the most massive galaxies (i.e. M1E11 and M1E12). This means that the role of the IMF slope in metal pollution is central: the top-heavier the IMF, the less ISM is trapped in low mass stars which do not contribute to the chemical enrichment. This gives the possibility to have a more rapid recycling of ISM. At the same time, the higher the SFR, the higher is the metal pollution in the ISM by dying stars: from the plot, however, we can say that SFR enhancement coming from flattening the IMF (see upper panel Figures 2, 3, 4) is a second order effect in getting the chemical enrichment faster. The discontinuities visible between $\sim 0.6 Gyr$ and $\sim 1.2 Gyr$ are due to the start of the galactic wind. As a matter of fact, the wind depletes the galaxy of its entire gas reservoir. At the same time, stars dying at that particular moment inject enriched material in the ISM. For this reason, [Fe/H] ratio jumps to the value obtained summing the yields of stars dying at that particular time.

Regarding the lower panel of Figure 5, it is evident that the flatter the IMF, the higher the [O/Fe] values at a given [Fe/H]. Moreover, the decline of [O/Fe] values happens at progressively higher Fe abundance values. This "delay" in the decline is much stronger for models adopting W11 IGIMF than more massive (M1E11, M1E12) models adopting the Salpeter (1955) IMF, which show however progressively larger [O/Fe] values at low metallicity. These behaviours are explained by the so called "time-delay model" (Matteucci 2003; 2012). [α/Fe] ratios tend to rise at low metallicity either if we increase the SFR or if we flatten the IMF: CC-SNe, whose number is strictly related to the

[2] [X/Y]=$\log(X/Y) - \log(X_{\odot}/Y_{\odot})$, where X, Y are abundances in the ISM for the object studied and $X_{\odot}$, $Y_{\odot}$ are solar abundances.

SFR and the slope of the IMF (Vincenzo et al. 2018), pollute the ISM mainly with α-elements, like O. The slower decline of [α/Fe] by IGIMF models, has to be attributed to two main factors. The first one is the different CC/Type Ia SN ratio. As explained in Section 3.2, the larger CC-SN rate caused by W11 IGIMF adoption does not correspond to a larger Type Ia SN rate. Massive stars are non negligible producers of Fe: in this way, the moment at which Type Ia SNe, producing mainly Fe, become important to chemical enrichment (i.e. the typical [α/Fe] knee) will be progressively shifted at higher Fe metallicities. The second factor is the much larger fraction of very massive stars ($m > 20 - 25 M_{\odot}$) in the top-heavy IGIMF adopted here (see Figure 1). Oxygen yields (e.g. Woosley & Weaver 1995; Thielemann et al. 1996; Kobayashi et al. 2006; Kobayashi et al. 2011) show in fact a dramatic increase at these masses with respect to less massive Type II SNe. This avoids the slow [O/Fe] decline at low metallicities in Salpeter (1955) IMF models, which is not caused by Type Ia SNe. To understand that, we can just look at the upper panel: at [Fe/H]$< -1.5\,dex$, we are well below the time at which the bulk of Type Ia SNe are produced.

We do not show them to avoid redundancies in the explanation, but we have to say that a similar general evolution characterises also the abundances of the $10^{11} M_{\odot}$ and $10^{12} M_{\odot}$ mass models adopting W11 IGIMF.

3.4 Abundances in high redshift starbursts

As we anticipated at the beginning of the Section, we will now compare the abundance patterns obtained by means of chemical evolution models adopting different IMF prescriptions with abundances obtained from spectra of high redshift starburst galaxies.

We will divide the discussion into two parts. First, we are treating the behaviour of elements like C, N and O, which are negligibly depleted in dust. Then, we see what happens in comparing data and models for refractory (i.e. considerably depleted in dust) elements, such as Fe, Mg and Si, either considering dust depletion or not. It is worth noting that we compare the results of specific models to specific galaxies: the criterion is to chose the model which predicts the SFR (the main feature driving chemical evolution) most similar to the observed one. For MS 1512-cB58 galaxy (for now on cB58, indicated with diamonds in the plots), we compare the observed abundances with both M3E10 and M1E11 models, due to the very different SFR values found in different studies adopting different SFR indicators (see Table 2).

3.4.1 Volatile elements

We start our analysis from the (N/O) vs. (O/H) ratios relation, visible in Figure 6. The analysis of elements such as N deserves a special attention, since still at present time the role of different stars in its production is not well understood.

For this reason, in the two plots of Figure 6 we show models with different N yields: the Matteucci (1986) (thick lines) and the Meynet & Maeder (2002) (thin lines) ones. The first

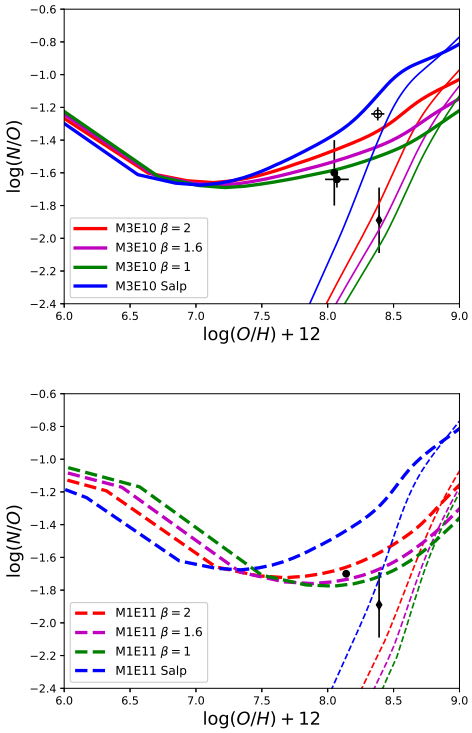

Figure 6. Predicted log(N/O) vs. log(O/H)+12 adopting Matteucci (1986) yields for N (thick lines) and Meynet & Maeder (2002) (thin lines) compared with abundances measured in galaxies of the sample of Table 2.
Upper panel: lines are computed for M3E10 models (solid) with Salpeter (1955) IMF (blue) and W11 IGIMF calculated for $\beta = 1$ (green), $\beta = 1.6$ (magenta) and $\beta = 2$ (red). Data are from Steidel et al. (2016) stacked spectum (empty circle), Bayliss et al. (2014), Christensen et al. (2012a, 2012b) (filled circles) and Pettini et al. (2002) (diamond).
Lower panel: lines are computed for M1E11 models (dashed) with a Salpeter (1955) IMF (blue) and W11 IGIMF calculated for $\beta = 1$ (green), $\beta = 1.6$ (magenta) and $\beta = 2$ (red). Data are from Rigby et al. (2011) (filled circle) and Pettini et al. (2002) (diamond).

set assume that all massive stars produce primary[3] N, an ad hoc hypothesis that is necessary to explain the relatively high (N/O) ratios observed in some low metallicity MW halo stars (Israelian et al. 2004; Spite et al. 2005). Meynet & Maeder (2002) yields, instead, allow for the production of primary N only rotating, massive, low metallicity stars. This behaviour, although physical, leads anyway to a deficiency of N between low and intermediate metallicities (Romano et al. 2010; Vincenzo et al. 2016), at variance with observations.

Coming back to the Figure, we see that the data have in general better agreement with models adopting Matteucci (1986) yields and the W11 IGIMF. The agreement with Meynet & Maeder (2002) scenario is in general worse, except for cB58 data, which instead agrees with IGIMF models (up-

[3] Production of an element directly from the synthesis of H and He. For secondary production, the seed for the synthesis must be a metal.

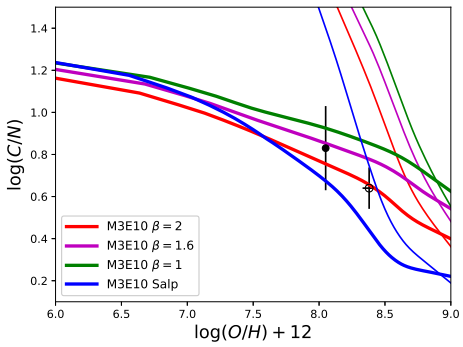

Figure 7. Predicted log(C/N) vs. log(O/H)+12 adopting Matteucci (1986) yields for N (thick lines) and Meynet & Maeder (2002) (thin lines) compared with abundances measured in galaxies of the sample of Table 2.
Lines are computed for M3E10 models (solid) with Salpeter (1955) IMF (blue) and W11 IGIMF calculated for $\beta = 1$ (green), $\beta = 1.6$ (magenta) and $\beta = 2$ (red). Data are from Steidel et al. (2016) stacked spectum (empty circle) and Bayliss et al. (2014) (filled circle).

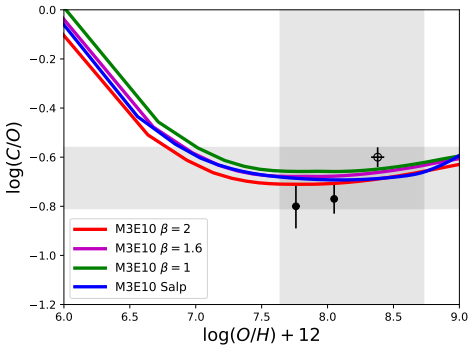

Figure 8. Predicted log(C/O) vs. log(O/H)+12 compared with abundances measured in galaxies of the sample of Table 2.
Lines are computed for M3E10 models (solid) with Salpeter (1955) IMF (blue) and W11 IGIMF calculated for $\beta = 1$ (green), $\beta = 1.6$ (magenta) and $\beta = 2$ (red). The shaded regions indicates the log(C/O) confidence region derived from the composite LBG spectrum of Shapley et al. (2003) and the log(O/H)+12 characterising the sample of LBGs of Pettini et al. (2001). Other data are from Steidel et al. (2016) stacked spectum (empty circle), Bayliss et al. (2014) and Christensen et al. (2012a, 2012b) (filled circles).

per panel, M3E10 models) or lies between Salpeter (1955) IMF and IGIMF models (lower panel, M1E11 models).

In Figure 7 we look at (C/N) vs. (O/H) relation. Here we have data for only two spectra. What is obtained here is in good agreement with what seen for (N/O) vs. (O/H) plots (except for cB58). The two data points are well explained by the patterns adopting Matteucci (1986) yields and W11 IGIMFs and the lower metallicity one in particular cannot be explained by any of the models adopting a scenario with mainly secondary production by massive stars.

The fact that most of the data are well explained by models adopting the top-heavy IGIMF of this paper is not surprising. In fact, several previous studies (e.g. Gibson & Matteucci 1997; Calura & Menci 2009) point out the necessity of a top-heavy IMF to explain elliptical galaxy data.

In Figure 8, we show the predicted behaviour of (C/O) vs. (O/H). We do not see here significant changes in varying the IMF. What we can say is that models fall in the confidence region derived by Shapley et al. (2003) stacked spectra and Pettini et al. (2001) sample of $z \sim 3$ LBGs. This general agreement can however be used as a proof for very massive stars ($m > 40 M_{\odot}$) rotation, necessary to increment C yields from these stars (e.g. Woosley & Weaver 1995): if we do not adopt this prescription, the resulting ratio will result too low to be consistent with the data.

However, a word of caution on our result is necessary: in particular, there are still uncertainties both in the models and the data. For the models, we have to consider the intrinsic uncertainties coming from stellar yields calculations. On the other side, in spite of the magnification given by lensing (or the stacking of spectra), the possibility of biases in the inferred abundances is not negligible. In fact, many parameters are necessary to obtain the abundance values, especially for emission line spectra (e.g. Kewley & Ellison 2008). The worst situation is for the O abundance obtained for cB58. As pointed out by Pettini et al. (2001), the possible log(O/H)+12 values span a range of $\sim 0.5 dex$, which can significantly alter our considerations on cB58.

3.4.2 Refractory elements

Figures 9 and 10 show the predicted [Si/Fe] and [Mg/Fe] vs. [Fe/H] without taking into account dust depletion effects, calculated for $10^{10} M_{\odot}$ and $10^{11} M_{\odot}$ models. The abundance patterns are compared with data measured in cB58 and 8 o'clock arc lensed LBGs. As explained in Section 3.4, we will compare the abundances measured in cB58 with both M3E10 and M1E11 models.

Looking at the upper panels of Figure 9 and 10, we do not see good agreement between M3E10 models and cB58 data. The situation is slightly better for the lower panels, showing M1E11 models and the M1E12 model with Salpeter (1955) IMF. Here, in fact, the models for lower β (and hence, top-heavier) IGIMFs fall inside the error bar of 8 o'clock data ([Si/Fe]) and reach the one of cB58 ([Mg/Fe]). All the models adopting a Salpeter (1955) IMF, even the one with the strongest star formation (with SFR values much higher than what observed in the considered galaxies), remain far away from the data. We should remark that, in spite of the uncertainties in the abundance determinations, it is quite evident that the models underestimate the observed [α/Fe] ratios, even when the top-heaviest IMFs are adopted.

For this reason we test also models considering elemental dust depletion. The models with dust are tracing separately the abundances in the gas and dust phases. It should be noted that this is the first time in which dust treatment is applied to chemical evolution models adopting an IGIMF. Previous chemical evolution studies including dust treatment (Pipino et al. 2011) failed in reproducing the abundances of cB58 adopting a Salpeter (1955) IMF, but they did not considered differential depletion, i.e. different elements depleted in dust in different proportions. In this work instead, we use elemental dust yields dependent on mass and metallicity of the stars, which allow us to treat the differential depletion of different elements. The results of models

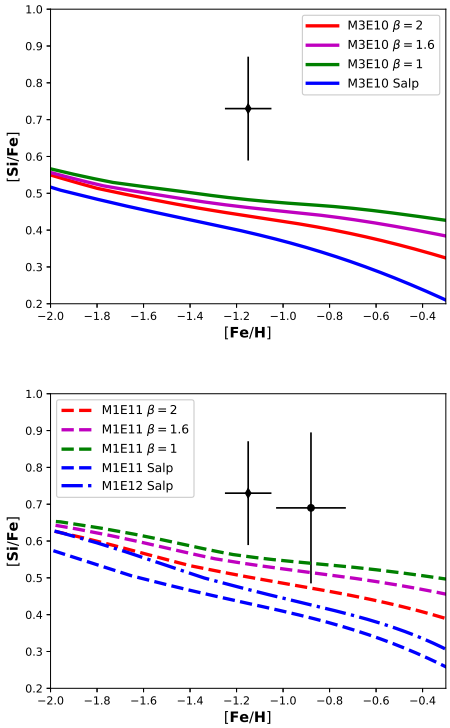

Figure 9. Predicted [Si/Fe] vs. [Fe/H] not accounting for dust depletion compared with abundances measured in galaxies of the sample of Table 2.
Upper panel: lines are computed for M3E10 models (solid) with Salpeter (1955) IMF (blue) and W11 IGIMF calculated for $\beta = 1$ (green), $\beta = 1.6$ (magenta) and $\beta = 2$ (red). Data are from Pettini et al. (2002) (diamond).
Lower panel:lines are computed for M1E11 models (dashed) with Salpeter (1955) IMF (blue), W11 IGIMF calculated for $\beta = 1$ (green), $\beta = 1.6$ (magenta) and $\beta = 2$ (red); M1E12 model with Salpeter (1955). Data are from Dessauges-Zavadsky et al. (2010) (filled circle) and Pettini et al. (2002) (diamond).

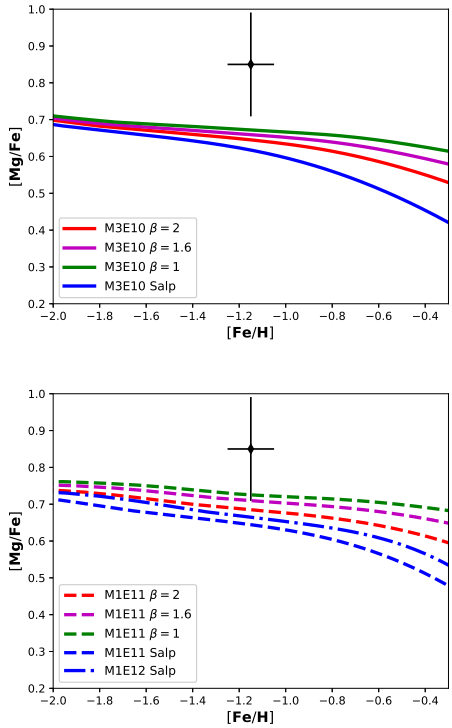

Figure 10. Predicted [Mg/Fe] vs. [Fe/H] not accounting for dust depletion compared with abundances measured in galaxies of the sample of Table 2.
Upper panel: lines are computed for M3E10 models (solid) with Salpeter (1955) IMF (blue) and W11 IGIMF calculated for $\beta = 1$ (green), $\beta = 1.6$ (magenta) and $\beta = 2$ (red). Data are from Pettini et al. (2002) (diamond).
Lower panel:lines are computed for M1E11 models (dashed) with Salpeter (1955) IMF (blue), W11 IGIMF calculated for $\beta = 1$ (green), $\beta = 1.6$ (magenta) and $\beta = 2$ (red); M1E12 model with Salpeter (1955). Data are from Pettini et al. (2002) (diamond).

considering dust are shown in Figures 11 and 12 for [Si/Fe] and [Mg/Fe] vs. [Fe/H], respectively.
We see in the Figures a much better agreement between data and models, both for [Si/Fe] and [Mg/Fe] ratios. With the exception of three of the four M3E10 models for [Si/Fe], almost all abundance patterns fall well inside data error bars. The main effect of dust depletion is to increase the [α/Fe] ratios because Fe is more depleted than α-elements. Lower panel of Figure 11 shows better agreement with data for [Si/Fe] patterns adopting W11 IGIMF, even with respect to the stronger star forming (but not correspondent to galaxies parameters) M1E12 model with a Salpeter (1955) IMF. This result obtained for [Si/Fe] vs. [Fe/H] support the evidences for a top-heavy IMF to explain observed [α/Fe] in ellipticals (e.g. Calura & Menci 2009; De Masi et al. 2018). However models including dust depletion do still slightly underestimate the observed abundance ratios. This can be attributed in large part to the uncertainties in dust production by Type II SNe, and in particular on the impact of the SN reverse shock on the survival of newly produced dust (see Gioannini et al. 2017). In addition to this, we also remind the large uncertainties that we have in the abundances measured for these high redshift objects (see 3.4.1). For these reasons, we consider the obtained agreement between data and models a good result. Furthermore, such a result was never reached by previous studies for the objects analysed in this work (e.g. Pipino et al. 2011).

4 CONCLUSIONS

In this work, we apply an integrated galactic IMF following Weidner et al. (2011) (W11) prescriptions to galactic chemical evolution models for high redshift starburst galaxies.

We study the effects of this IGIMF on the star formation history and chemical evolution of a given galaxy with respect to a classical Salpeter (1955) IMF.
In order to test the models and possibly find some constraints on the initial mass function in starburst galaxies, we compare the abundance patterns predicted by the models with the abundances observed in high redshift spectra of Lyman Break galaxies. In order to do this, we include in the models also a detailed dust treatment.

The results can be summarised as follows:

(i) We find a general increase of the rate of star formation

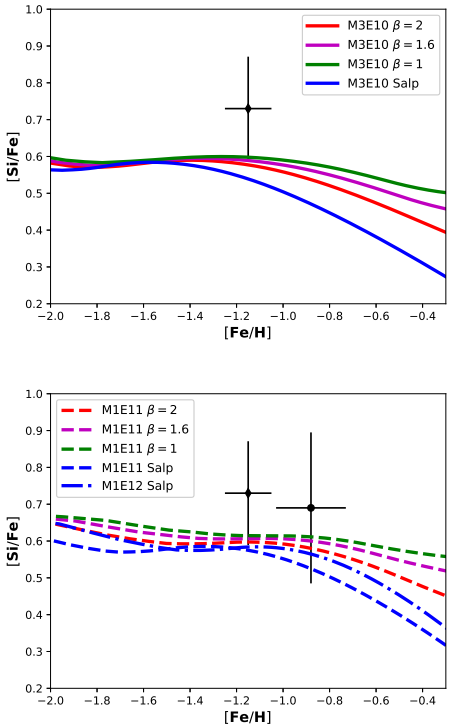

Figure 11. Same of Figure 9, but with models accounting for dust depletion effects.

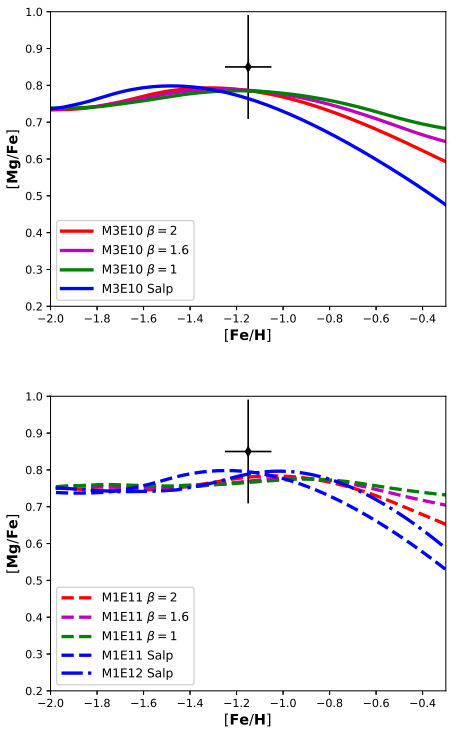

Figure 12. Same of Figure 10, but with models accounting for dust depletion effects.

in the models adopting the W11 IGIMF, with respect to the Salpeter (1955) IMF. In particular, we obtain higher SFRs by lowering the slope of the embedded cluster mass function β. This is the consequence of the IGIMF behaviour: the lower is β, the top-heavier (more massive stars) is the IMF. The massive stars, as soon as they die, restore gas to the galaxy, thus favouring star formation (SFR $\propto$ M_{gas}).
We find longer star formation histories (i.e. later galactic winds which end the burst of star formation) for lower β values (β = 1 in particular), whereas for the highest β adopted (= 2) we have times equal or lower than the ones obtained with a Salpeter (1955) IMF. This is probably due to the interplay between the SN rates (in particular, Type Ia rate) and the available gas mass in the galaxy. Indeed, the SN rates and the amount of gas influence the thermal energy and the binding energy of the galaxy, respectively (see De Masi et al. 2018 and references therein). These two quantities are crucial in determining the time of occurrence of the galactic wind (when $E_{thermal}$>E_{bind}) and the subsequent stop in the star formation.
In connection with the time of the wind occurrence, we see that the strong SFR dependence of the β = 1 IGIMF prevents to reproduce the inverse wind behaviour (Matteucci 1994; Thomas et al. 2002). For this reason, we think that the β = 1 IGIMF in models is unlikely. On the other hand, the cases for β > 1 are preserving the inverse wind situation and therefore should be preferred.

(ii) The different star formation histories obtained with different IMFs are reflected in the evolution of chemical abundances. The top-heavier is the IMF, the faster is the chemical enrichment. The central role in this is played by the IMF slope, which determines the fraction of low mass stars locking up the ISM, which otherwise could have been reprocessed.
At the same time, the lowering of β parameter in the IGIMF produces larger [α/Fe] values, with much prolonged plateaus as functions of [Fe/H]. This is simply linked to the different fraction of stars exploding as CC and Type Ia SNe, as explained by the "time-delay model" (Matteucci 2003; Matteucci 2012).

(iii) The comparison of the models with abundances taken from high redshift starbursts is not strongly conclusive on whether the W11 IGIMF can describe such systems better than a canonical Salpeter (1955) IMF. However, the analysis presented here definitively favors this top-heavy IGIMF.
Looking at volatile element abundance ratios, there is a good agreement between models adopting the IGIMF and the data, especially for the scenario of N primary production in massive stars. Uncertainties on the data and the stellar yields, however, do not exclude the possibility of having different explanations.
For what concerns refractory element abundances, the inclusion of a differential treatment of dust in the models allows us to reasonably reproduce the observed abundance ratios in cB58 and 8 o'clock arc LBGs. In any case, the data-model comparison gives much better results than what obtained by models without dust as well as by previous models not accounting for differential dust treatment (e.g. Pipino et al. 2011). [Si/Fe] patterns indicates much better accordance for models adopting W11 IGIMF with respect to the ones adopting Salpeter (1955) IMF. This supports the results obtained in previous studies (e.g. Gibson & Matteucci

1997; Zhang et al. 2018) that point out the necessity of a top-heavy IMF to deal with many of the elliptical galaxies observed features.

ACKNOWLEDGEMENTS

M. P., F. M. acknowledge financial support from the University of Trieste (FRA2016).

References

Asano R. S., Takeuchi T. T., Hirashita H., Inoue A. K., 2013, Earth, Planets, and Space, 65, 213
Bastian N., 2008, MNRAS, 390, 759
Baugh C. M., Lacey C. G., Frenk C. S., Granato G. L., Silva L., Bressan A., Benson A. J., Cole S., 2005, MNRAS, 356, 1191
Bayliss M. B., Rigby J. R., Sharon K., Wuyts E., Florian M., Gladders M. D., Johnson T., Oguri M., 2014, ApJ, 790, 144
Bianchi S., Schneider R., 2007, MNRAS, 378, 973
Bradamante F., Matteucci F., D'Ercole A., 1998, A&A, 337, 338
Calura F., Matteucci F., 2006, ApJ, 652, 889
Calura F., Menci N., 2009, MNRAS, 400, 1347
Calura F., Pipino A., Matteucci F., 2008, A&A, 479, 669
Calura F., Recchi S., Matteucci F., Kroupa P., 2010, MNRAS, 406, 1985
Calura F., Gilli R., Vignali C., Pozzi F., Pipino A., Matteucci F., 2014, MNRAS, 438, 2765
Cenarro A. J., Gorgas J., Vazdekis A., Cardiel N., Peletier R. F., 2003, MNRAS, 339, L12
Christensen L., et al., 2012a, MNRAS, 427, 1953
Christensen L., et al., 2012b, MNRAS, 427, 1973
Cioffi D. F., McKee C. F., Bertschinger E., 1988, ApJ, 334, 252
Conroy C., van Dokkum P., 2012a, ApJ, 747, 69
Conroy C., van Dokkum P. G., 2012b, ApJ, 760, 71
D'Antona F., Caloi V., 2004, ApJ, 611, 871
D'Ercole A., Vesperini E., D'Antona F., McMillan S. L. W., Recchi S., 2008, MNRAS, 391, 825
Davé R., 2008, MNRAS, 385, 147
De Masi C., Matteucci F., Vincenzo F., 2018, MNRAS, 474, 5259
Dell'Agli F., García-Hernández D. A., Schneider R., Ventura P., La Franca F., Valiante R., Marini E., Di Criscienzo M., 2017, MNRAS, 467, 4431
Dessauges-Zavadsky M., D'Odorico S., Schaerer D., Modigliani A., Tapken C., Vernet J., 2010, A&A, 510, A26
Dwek E., 1998, ApJ, 501, 643
Ferreras I., Weidner C., Vazdekis A., La Barbera F., 2015, MNRAS, 448, L82
Finkelstein S. L., Papovich C., Rudnick G., Egami E., Le Floc'h E., Rieke M. J., Rigby J. R., Willmer C. N. A., 2009, ApJ, 700, 376
François P., Matteucci F., Cayrel R., Spite M., Spite F., Chiappini C., 2004, A&A, 421, 613
Gibson B. K., Matteucci F., 1997, MNRAS, 291, L8
Ginolfi M., Graziani L., Schneider R., Marassi S., Valiante R., Dell'Agli F., Ventura P., Hunt L. K., 2018, MNRAS, 473, 4538
Gioannini L., Matteucci F., Vladilo G., Calura F., 2017, MNRAS, 464, 985
Gomez H. L., et al., 2012, ApJ, 760, 96
Grieco V., Matteucci F., Calura F., Boissier S., Longo F., D'Elia V., 2014, MNRAS, 444, 1054
Israelian G., Ecuvillon A., Rebolo R., García-López R., Bonifacio P., Molaro P., 2004, A&A, 421, 649
Iwamoto K., Brachwitz F., Nomoto K., Kishimoto N., Umeda H., Hix W. R., Thielemann F.-K., 1999, ApJS, 125, 439
Kennicutt Jr. R. C., 1998, ApJ, 498, 541
Kewley L. J., Ellison S. L., 2008, ApJ, 681, 1183
Kobayashi C., Umeda H., Nomoto K., Tominaga N., Ohkubo T., 2006, ApJ, 653, 1145
Kobayashi C., Karakas A. I., Umeda H., 2011, MNRAS, 414, 3231
Kroupa P., 2001, MNRAS, 322, 231
Kroupa P., 2002, Science, 295, 82
Kroupa P., Weidner C., 2003, ApJ, 598, 1076
La Barbera F., Ferreras I., Vazdekis A., de la Rosa I. G., de Carvalho R. R., Trevisan M., Falcón-Barroso J., Ricciardelli E., 2013, MNRAS, 433, 3017
Lada C. J., Lada E. A., 2003, ARA&A, 41, 57
Larson R. B., 1998, MNRAS, 301, 569
Marks M., Kroupa P., Dabringhausen J., Pawlowski M. S., 2012, MNRAS, 422, 2246
Massey P., Hunter D. A., 1998, ApJ, 493, 180
Matteucci F., 1986, MNRAS, 221, 911
Matteucci F., 1994, A&A, 288, 57
Matteucci F., 2003, The Chemical Evolution of the Galaxy
Matteucci F., 2012, Chemical Evolution of Galaxies, doi:10.1007/978-3-642-22491-1.
Matteucci F., Greggio L., 1986, A&A, 154, 279
Matteucci F., Pipino A., 2002, ApJ, 569, L69
Matteucci F., Recchi S., 2001, ApJ, 558, 351
Meynet G., Maeder A., 2002, A&A, 390, 561
Nozawa T., Maeda K., Kozasa T., Tanaka M., Nomoto K., Umeda H., 2011, ApJ, 736, 45
Palla M., Matteucci F., Calura F., Longo F., 2019, preprint, (arXiv:1903.01353)
Pettini M., Steidel C. C., Adelberger K. L., Dickinson M., Giavalisco M., 2000, ApJ, 528, 96
Pettini M., Shapley A. E., Steidel C. C., Cuby J.-G., Dickinson M., Moorwood A. F. M., Adelberger K. L., Giavalisco M., 2001, ApJ, 554, 981
Pettini M., Rix S. A., Steidel C. C., Adelberger K. L., Hunt M. P., Shapley A. E., 2002, ApJ, 569, 742
Pflamm-Altenburg J., Weidner C., Kroupa P., 2007, ApJ, 671, 1550
Pipino A., Matteucci F., 2004, MNRAS, 347, 968
Pipino A., Matteucci F., 2011, A&A, 530, A98
Pipino A., Fan X. L., Matteucci F., Calura F., Silva L., Granato G., Maiolino R., 2011, A&A, 525, A61
Recchi S., Matteucci F., D'Ercole A., 2001, MNRAS, 322, 800
Recchi S., Calura F., Kroupa P., 2009, A&A, 499, 711
Recchi S., Calura F., Gibson B. K., Kroupa P., 2014, MNRAS, 437, 994

Rigby J. R., Wuyts E., Gladders M. D., Sharon K., Becker G. D., 2011, ApJ, 732, 59
Romano D., Karakas A. I., Tosi M., Matteucci F., 2010, A&A, 522, A32
Salpeter E. E., 1955, ApJ, 121, 161
Schmidt M., 1959, ApJ, 129, 243
Shapley A. E., Steidel C. C., Pettini M., Adelberger K. L., 2003, ApJ, 588, 65
Siana B., Teplitz H. I., Chary R.-R., Colbert J., Frayer D. T., 2008, ApJ, 689, 59
Spite M., et al., 2005, A&A, 430, 655
Steidel C. C., Strom A. L., Pettini M., Rudie G. C., Reddy N. A., Trainor R. F., 2016, ApJ, 826, 159
Teplitz H. I., et al., 2000, ApJ, 533, L65
Thielemann F.-K., Nomoto K., Hashimoto M.-A., 1996, ApJ, 460, 408
Thomas D., Maraston C., Bender R., 2002, Ap&SS, 281, 371
Vincenzo F., Matteucci F., Recchi S., Calura F., McWilliam A., Lanfranchi G. A., 2015, MNRAS, 449, 1327
Vincenzo F., Belfiore F., Maiolino R., Matteucci F., Ventura P., 2016, MNRAS, 458, 3466
Vincenzo F., Kobayashi C., Taylor P., 2018, MNRAS, 480, L38
Vladilo G., Gioannini L., Matteucci F., Palla M., 2018, ApJ, 868, 127
Weidner C., Kroupa P., 2004, MNRAS, 348, 187
Weidner C., Kroupa P., 2005, ApJ, 625, 754
Weidner C., Kroupa P., Pflamm-Altenburg J., 2011, MNRAS, 412, 979
Weidner C., Ferreras I., Vazdekis A., La Barbera F., 2013, MNRAS, 435, 2274
Woosley S. E., Weaver T. A., 1995, ApJS, 101, 181
Wuyts E., et al., 2010, ApJ, 724, 1182
Yan Z., Jerabkova T., Kroupa P., Vazdekis A., 2019, preprint, (arXiv:1907.10614)
Zhang Z.-Y., Romano D., Ivison R. J., Papadopoulos P. P., Matteucci F., 2018, Nature, 558, 260
van den Hoek L. B., Groenewegen M. A. T., 1997, A&AS, 123, 305

This paper has been typeset from a TEX/LATEX file prepared by the author.